arXiv:1212.6181v2 [quant-ph] 27 Dec 2012

A circuit QED architecture with current-biased flux qubits

Mun Dae Kim
Institute for Mathematical Science, Yonsei University, Seoul 120-749, Korea and
Korea Institute for Advanced Study, Seoul 130-722, Korea

(Dated: January 1, 2013)

We theoretically study a circuit quantum electrodynamics (QED) architecture with current-biased flux qubits. The qubit is coupled to the transmission line resonator by a bias current originating from the current mode of the resonator. Ultrastrong coupling regime can be obtained by varying the capacitance between the qubit and the resonator. We propose a scalable design for the circuit QED with current-biased flux qubits, where the dc-SQUIDs take the role of switching the qubit-resonator coupling. An exact calculation on two-qubit coupling strength in the scalable design shows the transition from ferromagnetic to antiferromagnetic xy-type interaction.

PACS numbers: 74.50.+r, 03.67.Lx, 85.25.Cp

I. INTRODUCTION

An artificial two level system can be coupled with the quantized electromagnetic field in a superconducting transmission line resonator, while the natural atom is coupled with 3D cavity. This circuit quantum electrodynamics (QED) architecture[1,2] is a solid-state analog of 3D cavity QED, providing a strong coupling strength between the qubit and resonator owing to the large dipole moment of the artificial qubit. The circuit QED scheme has been applied to the superconducting qubits. Among the superconducting qubits the flux qubit[3–5] has the advantage of fast gate operation because the flux qubit does not require low anharmonicity in circuit QED scheme. There have been many studies for the circuit QED with the superconducting flux qubit.[9,10] However, the inductive coupling between the flux qubit and the transmission line resonator of the circuit is too weak to perform the quantum gate operation.

Recently a galvanic coupling scheme for the circuit QED with the flux qubits has been proposed to enhance the coupling strength by sharing the flux qubit loop and the resonator transmission line.[6–8] In this study, we propose a *bias current coupling* scheme between the flux qubit and the transmission line resonator; the qubit and the resonator are not galvanically coupled with each other, but by a current flowing through the capacitance between the qubit and the resonator. In this scheme the three-junctions flux qubit is coupled by a bias current similarly to the superconducting phase qubit.[11–14] While the states of phase qubit are defined in terms of the phase degrees of freedom in a washboard type potential, the present current-biased flux qubit uses the persistent current states as qubit states. The qubit state preparation and the quantum gate operation are achieved by the bias current. Our qubit thus has the advantages of phase qubit such as fast qubit operation and readout and individual addressing.

In the design of our qubit the capacitance can be controlled by varying the width of capacitance line extended from the qubit loop and the distance between the capacitance line and the transmission line resonator. The coupling strength between the qubit and the resonator shows a maximum where the coupling constant can reach even ultrastrong coupling regime with reasonable parameter values.

We also introduce a scalable design with switching function and study the behavior of coupling strength for various number of qubits. The coupling between qubit and the resonator can be switched on/off by using a dc-SQUID inserted between the flux qubit and the ground plane of circuit QED. Further we analyze the xy-type interaction between two qubits. The two-qubit coupling is shown also to be strong, which requires an exact, not perturbative, representation of the two-qubit interaction. The obtained two-qubit coupling shows that we can selectively choose between ferromagnetic and antiferromagnetic xy-type coupling by varying system parameters.

II. A STRONG COUPLING AND SINGLE QUBIT OPERATION

A. Strong qubit-resonator coupling

Usually the transmon qubit is coupled with the voltage mode of the transmission line resonator through a capacitance.[1,2] For superconducting flux qubits, there have been many studies to couple the flux qubit with the transmission line resonator by using mutual inductance between the qubit loop and the resonator[9,10] or by sharing the qubit loop with the resonator.[6–8] On the other hand the three-junctions flux qubit can also be coupled with the transmission line resonator through a capacitance, but in this case it is coupled with the *current mode* of the resonator. An oscillating bias current flowing across the capacitance gives rise to the coupling between the qubit and the resonator.[15]

If the three-junctions flux qubit is penetrated by a magnetic flux of half flux quantum $\Phi_0/2$, there are two current states in the qubit loop. The clockwise and counterclockwise current states correspond to the local minima in the effective potential of the qubit loop. If the three Josephson junctions are identical, they have equal phase difference $\pm\alpha$ with $\alpha = \pi/3$, depending on the current states. When a bias current I_0 is applied to the flux qubit where three Josephson junctions are located asymmetrically in the loop as shown in Fig. 1, the coupling strength is given by a product of flux variable and bias current[15]

$$g = \frac{\Phi_0}{2\pi}\alpha I_0 \tag{1}$$

similarly to the superconducting phase qubit.[13,16] Here we have the phase difference α instead of 3α because the two phases in different sides of the qubit are cancelled out each other. This bias current coupling has recently been realized in experiments with three-junctions flux qubit.[17–19]

In this study, we consider a qubit design which can control the capacitance between the qubit and the resonator. Large capacitance allows high bias current, and thus makes the qubit-resonator coupling reach even ultrastrong coupling regime. We consider a qubit design shown in Fig. 1(a), where the three-junctions flux qubit is coupled with the transmission line resonator by a capacitance line extended from the qubit loop. The width w of the capacitance line and the distance d between the capacitance line and the resonator can be adjusted to determine the capacitance between the qubit and the resonator. In this case the capacitance density around the qubit location is larger than other area of the resonator, providing a strong qubit-resonator coupling. Two capacitors at the ends of the resonator are introduced for the current mode of the resonator to be periodic in a scalable design. Here we use the second harmonics of the current mode, and the arrows show the corresponding current in the circuit.

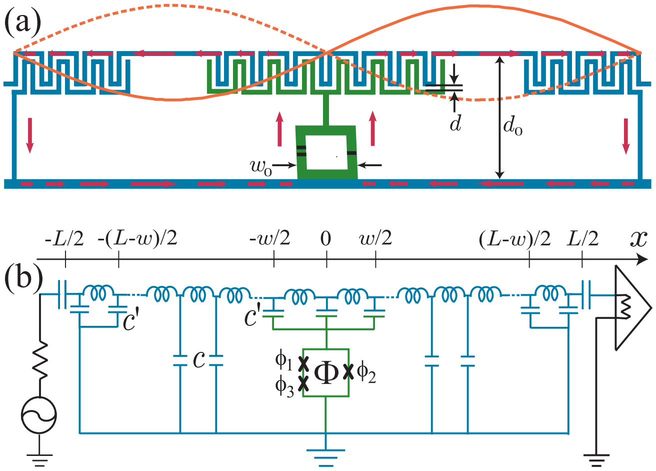

FIG. 1: (a) A current-biased three-junctions flux qubit where w_0 is the width of qubit loop and d_0 the distance between the resonator and the ground plane. The upper superconducting plane is the transmission line resonator and the lower is the ground plane. (b) A schematic diagram for the circuit in (a), where c and c' are the capacitance density. The three Josephson junctions with phase difference ϕ_i are located asymmetrically along the qubit loop with threading flux Φ.

The microwave passing through the uniform resonator in the circuit QED architecture can be described as a one-dimensional motion by the Lagrangian

$$\mathcal{L}(\theta, \dot{\theta}; t) = \int_{-\frac{L}{2}}^{\frac{L}{2}} \left(\frac{l}{2}(\dot{\theta}(x,t))^2 - \frac{1}{2c}(\nabla\theta(x,t))^2 \right) dx, \tag{2}$$

where l and c are the inductance and the capacitance per unit length of the uniform transmission line resonator, respectively, and $\theta(x,t) = \int_{-L/2}^{x} dx' q(x',t)$ with the linear charge density $q(x)$ is a collective field variable.

Figure 1(b) shows the schematic diagram of (a), where c and c' are the capacitance density between the resonator and the ground plane and between the resonator and the qubit, respectively. When $c' \gg c$, almost current flows through the qubit at the center and the capacitors at the ends of the resonator. The resonator thus is not uniform any more, and the equation of motion of the field variable in the sector i of the resonator is given by in terms of the Euler-Lagrange equation

$$\frac{1}{c_i}\frac{\partial^2\theta_i(x,t)}{\partial x^2} - l\frac{\partial^2\theta_i(x,t)}{\partial t^2} = 0. \tag{3}$$

If the field variable is represented as a product of spatial and temporal parts $\theta_i(x,t) = X_i(x)\phi(t)$, we get the equation

$$\frac{1}{c_i}\frac{\partial^2}{\partial x^2}X_i(x) + l\omega_r^2 X_i(x) = 0. \tag{4}$$

The spatial part $X_i(x)$ $(-2 \le i \le 2)$ is explicitly written as

$$X(x) = \begin{cases} A_{-2}e^{i\frac{j_2\pi}{L}x} + B_{-2}e^{-i\frac{j_2\pi}{L}x} & (-\frac{L}{2} < x < -\frac{L}{2} + \frac{w}{2}) \\ A_{-1}e^{i\frac{j_1\pi}{L}x} + B_{-1}e^{-i\frac{j_1\pi}{L}x} & (-\frac{L}{2} + \frac{w}{2} < x < -\frac{w}{2}) \\ A_0 e^{i\frac{j_2\pi}{L}x} + B_0 e^{-i\frac{j_2\pi}{L}x} & (-\frac{w}{2} < x < \frac{w}{2}) \\ A_1 e^{i\frac{j_1\pi}{L}x} + B_1 e^{-i\frac{j_1\pi}{L}x} & (\frac{w}{2} < x < \frac{L}{2} - \frac{w}{2}) \\ A_2 e^{i\frac{j_2\pi}{L}x} + B_2 e^{-i\frac{j_2\pi}{L}x} & (\frac{L}{2} - \frac{w}{2} < x < \frac{L}{2}) \end{cases} \tag{5}$$

and $\omega_r = \frac{1}{\sqrt{lc_i}}\frac{j_i\pi}{L}$ is the resonator frequency. Here $c_i = c$ and $j_i = j_1$ for odd i and $c_i = c'$ and $j_i = j_2$ for even i, and thus we have

$$\frac{1}{\sqrt{lc}}\frac{j_1\pi}{L} = \frac{1}{\sqrt{lc'}}\frac{j_2\pi}{L} = \omega_r. \tag{6}$$

From Eq. (4) we can readily observe that $(1/c_i)\partial X_i(x)/\partial x$ and $X_i(x)$ are continuous at the boundary between the sectors, which means the continuity of electric potential $V_i(x,t) = (1/c_i)\partial\theta(x,t)/\partial x = (1/c_i)\nabla X_i(x)\phi(t)$ and current $I(x,t) = \partial\theta(x,t)/\partial t = X(x)\dot{\phi}(t)$ at boundary. In Fig. 1 the resonator and the qubit are coupled by a bias current flowing into the qubit through the capacitance in the region $-w/2 < x < w/2$. The bias current is given by

$$I_b(t) = \int_{-w/2}^{w/2} \dot{q}(x,t)dx = I\left(\frac{w}{2},t\right) - I\left(-\frac{w}{2},t\right) \qquad (7)$$

from the current conservation condition $\dot{q}(x,t) = \partial I(x,t)/\partial x$ in the resonator. The other current flows from the resonator to the ground plane directly through the capacitors with small capacitance density c in Fig. 1(b).

In Appendix A we present the boundary conditions for general N qubit case. We, first of all, consider $N = 1$ case. The boundary conditions are categorized into two sets in Appendix A. $X(x)$ should be an odd function in order to have a finite coupling constant g, because the bias current of Eq. (7) vanishes if $X(x)$ is an even function for $-w/2 < x < w/2$. In Appendix A, thus, the determinant of matrix corresponding to set (ii) of boundary conditions should be zero, resulting in

$$e^{\frac{ij_1\pi}{2}\left(1-\frac{2w}{L}\right)} = \pm\frac{cj_2\cos\frac{j_2\pi}{2}\frac{w}{L} - ic'j_1\sin\frac{j_2\pi}{2}\frac{w}{L}}{cj_2\cos\frac{j_2\pi}{2}\frac{w}{L} + ic'j_1\sin\frac{j_2\pi}{2}\frac{w}{L}}. \qquad (8)$$

The values of j_1, j_2 and ω_r are determined from Eqs. (6) and (8). For uniform capacitance density $c' = c$, j_1 and j_2 are integers, but in general they are rational numbers depending on the ratio c'/c.

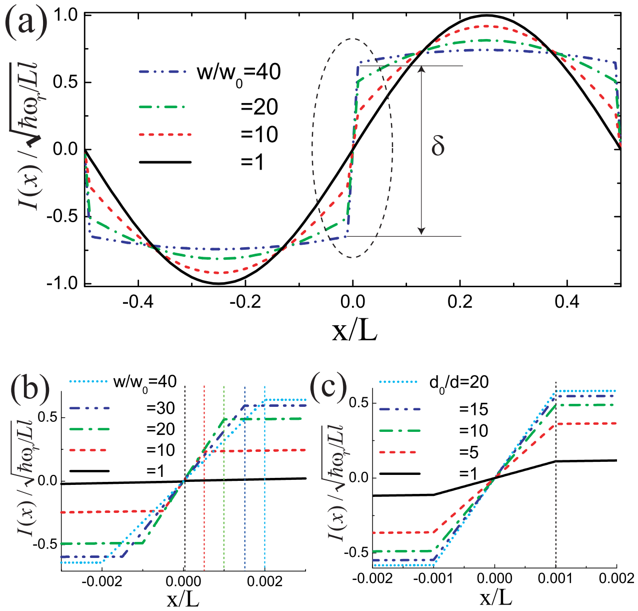

FIG. 2: (a) Current profile of single qubit case for various w/w_0 with $d_0/d = 10$ and $w_0/L = 10^{-4}$. The gap δ around $x/L = 0$ increases along with w/w_0, which gives rise to a strong coupling constant g. (b) The enlarged current profile around the gap inside the dotted ellipse in (a) for various w/w_0 with $d_0/d = 10$ and (c) for various d_0/d with w/w_0=20. Thin dotted lines indicate the boundary position $x = w/2$, the end of the capacitance line. As w/w_0 and d_0/d increase, the gap grows and is finally saturated.

The set (i) of boundary conditions in Appendix A provides the relation $A_{-i} = -B_i$, and the coefficients A_i and B_i are determined from the set (ii) of boundary conditions as

$$\begin{aligned}
B_2 &= -e^{ij_2\pi}A_2,\\
A_1 &= -\frac{1}{j_1}e^{\frac{i\pi}{2}\left(j_2-j_1\left(1-\frac{w}{L}\right)\right)}\left(-\frac{cj_2}{c'}\cos\frac{j_2\pi}{2}\frac{w}{L}+ij_1\sin\frac{j_2\pi}{2}\frac{w}{L}\right)A_2,\\
B_1 &= -\frac{1}{j_1}e^{\frac{i\pi}{2}\left(j_2+j_1\left(1-\frac{w}{L}\right)\right)}\left(\frac{cj_2}{c'}\cos\frac{j_2\pi}{2}\frac{w}{L}+ij_1\sin\frac{j_2\pi}{2}\frac{w}{L}\right)A_2,\\
A_0 &= \frac{c'j_1}{2cj_2\cos\frac{j_2\pi}{2}\frac{w}{L}}\left(e^{i\frac{j_1\pi}{2}\frac{w}{L}}A_1 - e^{-i\frac{j_1\pi}{2}\frac{w}{L}}B_1\right). \qquad (9)
\end{aligned}$$

The Lagrangian in Eq. (2) of the resonator modes can be written as $\mathcal{L}(\phi,\dot{\phi}) = L\left(\frac{l}{2}\mu\dot{\phi}^2 - \frac{1}{2c}\kappa\phi^2\right)$ with dimensionless constant $\mu = (1/L)\sum_i\int_{-L/2}^{L/2}X_i^2(x)dx$ and $\kappa = (1/L)\sum_i\int_{-L/2}^{L/2}(c/c_i)(\nabla X_i(x))^2dx$. If we introduce the representations [1]

$$\dot{\phi}(t) = \frac{-i}{\sqrt{2\mu}}\sqrt{\frac{\hbar\omega_r}{Ll}}(a - a^\dagger), \qquad (10)$$

$$\phi(t) = \frac{1}{\sqrt{2\kappa}}\sqrt{\frac{\hbar\omega_r c}{L}}(a + a^\dagger), \qquad (11)$$

the Hamiltonian of the resonator modes is written in a diagonalized form $H_r = \hbar\omega_r(a^\dagger a + \frac{1}{2})$. The current $I(x,t) = X(x)\dot{\phi}(t)$ is then given by

$$I(x,t) = -i\frac{X(x)}{\sqrt{2\mu}}\sqrt{\frac{\hbar\omega_r}{Ll}}(a - a^\dagger), \qquad (12)$$

where the remaining coefficient A_2 in Eq. (9) is a common factor in the numerator and denominator, and thus is cancelled out.

The total Hamiltonian $H_{\rm JC} = H_r + H_q + H_I$ given by the sum of the Hamiltonian for the resonator modes, for the qubit, and for the interaction between the resonator modes and the qubit is written as a Jaynes-Cummings type Hamiltonian[15]

$$H_{\rm JC} = \hbar\omega_r a^\dagger a + \frac{\omega_a}{2}\sigma_z + ig\sigma_x(a - a^\dagger), \qquad (13)$$

where ω_a is the qubit frequency and the last term represents the coupling between the qubit and the current mode in the resonator, which is different from $g\sigma_x(a+a^\dagger)$ in transmon case. This type of bias current coupling term for the three-junctions flux qubit has also been derived recently in a different manner.[19]

The amplitude of bias current in Eq. (7) is given by

$$I_0 = \sqrt{\frac{\hbar\omega_r}{Ll}}\delta \qquad (14)$$

with

$$\delta = 2\frac{X(\frac{w}{2})}{\sqrt{2\mu}}, \tag{15}$$

and thus the coupling strength g in Eq. (1) is determined by δ and ω_r. Since the amplitude of current $I(x,t)$ in Eq. (12) satisfies the condition, $(1/L)\sum_i \int_{-L/2}^{L/2}(X_i(x)/\sqrt{2\mu})^2 dx = 0.5$, δ has the maximum value of $\sqrt{2}$ when the current profile takes the rectangular function form.

In Fig. 2 (a) we show the current profile $I(x) = \frac{X(x)}{\sqrt{2\mu}}\sqrt{\frac{\hbar\omega_r}{Ll}}$, where we set $w_0/L = 10^{-4}$ corresponding to $w_0 = 1\mu$m when $L = 10$mm. Here a finite current gap develops around the qubit location at the center of the resonator. The capacitance $c' = (wd_0/w_0 d)c$ between the resonator and the capacitance line increases along with w/w_0 and d_0/d, which enables more charges to flow across the qubit. The resulting large bias current, producing the gap in current profile of Fig. 2(a), gives rise to a strong coupling g.

Fig. 2(b) shows the central part of current profile closed by a dotted ellipse in Fig. 2(a) for various w/w_0 with fixed d_0/d, demonstrating a larger gap for larger w/w_0. At the boundary ($x = \pm w/2$), the electric potential $(1/c_i)\partial X_i(x)/\partial x$ is continuous. Fig. 2(c) shows the currents for various d_0/d with fixed w/w_0, which shows the gap also grows along with d_0/d. These figures show that the current gap δ grows along with both w/w_0 and d_0/d, and is finally saturated to $\sqrt{2}$.

The coupling constant in Eq. (1) can be rewritten as

$$\frac{g}{\hbar\omega_r^0} = \frac{1}{3}\frac{\Phi_0}{\sqrt{hZ}}\sqrt{\frac{\omega_r}{\omega_r^0}}\frac{\delta}{\sqrt{2}}, \tag{16}$$

where $\omega_r^0 = \pi/\sqrt{lc}L$ is the frequency of the 1st harmonic mode of the uniform resonator as can be seen in Eq. (6) and $Z = \sqrt{l/c}$ is the impedance of the resonator.[20] In Fig. 3 we show the coupling constant g in the plane of $(d_0/d,\ w/w_0)$ with $Z = 50\Omega$.[6,10] From the contour plot of the g at the bottom of the figure the strong coupling regime ($g \sim \hbar\omega_r^0$) is shown to be achievable with w and $1/d$ of just several multiples of w_0 and $1/d_0$. The coupling g shows a maximum, where the coupling reaches ultrastrong coupling regime.

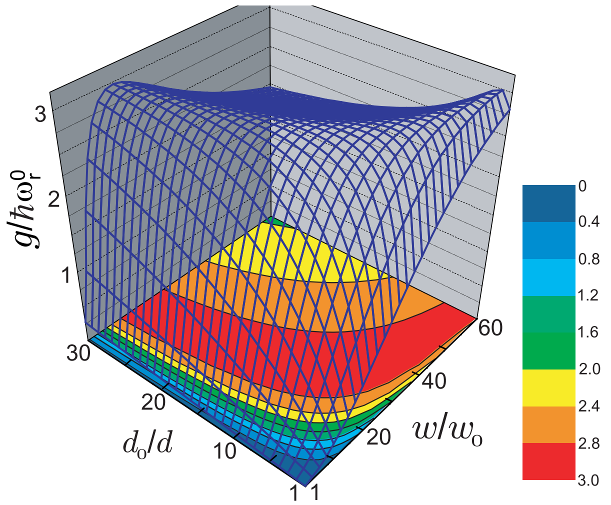

FIG. 3: Coupling constant g for the single qubit case in the plane of $(d_0/d, w/w_0)$ with the resonator impedance $Z = 50\Omega$. g has a maximum value corresponding to a ultrastrong coupling. At the bottom the contour plot of g is shown.

In Fig. 5 the behaviors of the current gap δ, the resonator frequency ω_r, and the coupling g along the diagonal line $w/w_0 = 2d_0/d$ in the plane of $(w/w_0,\ d_0/d)$ in Fig. 3 are shown. Note that the frequency of the resonator mode ω_r^0 becomes small for large c. The increase of w/w_0 and d_0/d makes the average capacitance of the resonator larger, and thus the resonator frequency ω_r smaller. As a result, the coupling g in Eq. (16) demonstrates a global maximum because ω_r decreases while δ increases.

B. Single qubit gate

Single qubit gate can be performed by applying an external driving mode $H_D = \epsilon a^\dagger e^{-i\omega_d t} + \epsilon^* a e^{i\omega_d t}$. The total Hamiltonian is written as $H_t = H_{\rm JC}^R + H_D$, where $H_{\rm JC}^R$ is given in the rotating wave approximation (RWA) of the Hamiltonian in Eq. (13). By using the transformation[2] $\mathcal{D}(\gamma) = e^{\gamma a^\dagger - \gamma^* a}$ with $\gamma(t) = -(\epsilon/\Delta_r)e^{-i\omega_d t}$ and $\Delta_r = \omega_r - \omega_d$, we can get the transformed Hamiltonian $\tilde{H} = \mathcal{D}^\dagger H_t \mathcal{D} - i\mathcal{D}^\dagger\dot{\mathcal{D}}$ given by

$$\tilde{H} = \Delta_r a^\dagger a + \frac{\Delta_a}{2}\sigma_z - ig(a^\dagger\sigma_- - a\sigma_+) + \frac{\Omega_R}{2}\sigma_y \tag{17}$$

with $\Delta_a = \omega_a - \omega_d$.

This Hamiltonian can be considered as if it is derived from the RWA of the Hamiltonian $H_t' = \Delta_r a^\dagger a + \frac{\Delta_a}{2}\sigma_z - g(a + a^\dagger)\sigma_y + \frac{\Omega_R}{2}\sigma_y$, which is identical to the Hamiltonian for the circuit QED with transmon qubit in Ref. [2] except σ_y instead of σ_x. Hence the analysis of qubit operation for our current-biased flux qubit can be obtained from Ref. [2] by simply replacing σ_x with σ_y. In the dispersive regime $|\Delta| \gg g$ with $\Delta = \omega_a - \omega_r$, for example, the coupling between qubit and resonator can be eliminated by introducing the transformation $\mathcal{H} = \mathcal{U}^\dagger\tilde{H}\mathcal{U}$ with $\mathcal{U} = e^{-i\frac{g}{\Delta}(a^\dagger\sigma_- + a\sigma_+)}$, resulting in

$$\mathcal{H} \approx \Delta_r a^\dagger a + \frac{\Delta_a}{2}\sigma_z + \chi(a^\dagger a + \frac{1}{2})\sigma_z + \frac{\Omega_R}{2}\sigma_y \tag{18}$$

with $\chi = g^2/\Delta$. This Hamiltonian shows the resonator transmission shift $\pm\chi$ depending on the qubit state.

For the present current-biased flux qubit we can get much stronger coupling $g \gtrsim \Delta$. In this case we cannot use above small parameter expansion any more, and thus should calculate exact energy eigenvalues by diagonalizing the Hamiltonian in the RWA

$$H_n^R = \begin{pmatrix} (n+1)\Delta_r - \frac{\Delta_a}{2} & -ig\sqrt{n+1} \\ ig\sqrt{n+1} & n\Delta_r + \frac{\Delta_a}{2} \end{pmatrix}, \tag{19}$$

which results in the eigenvalues

$$E_n = \pm\sqrt{\left(\frac{\Delta}{2}\right)^2 + (n+1)g^2}. \tag{20}$$

For weak coupling regime $g \ll \Delta$ with the photon number $n = 0$ in the resonator we have $E_n \approx \pm[(\omega_a - \omega_r)/2 + g^2/\Delta]$, where the first term is the energy for the qubit and resonator, and the second term corresponds to the frequency shift of $\pm\chi$.

III. A SCALABLE DESIGN AND TWO-QUBIT COUPLING

A. Scalable design

Figure 4(a) shows the schematic diagram of a scalable design for the circuit QED with current-biased flux qubits, where dc-SQUIDs are inserted between the qubit and the ground plane for switching the qubit-resonator coupling. Φ_{xi} and Φ_{si} are the external and switching flux for i-th qubit, respectively. Usually superconducting qubits are coupled with the resonator by the voltage mode or the mutual inductance. The current-biased flux qubit, however, is coupled with the resonator through the current flowing across the capacitance between the qubit and the resonator. Hence, if we switch off the bias current by piercing a half-flux quantum into the dc-SQUID loop, the qubit and the resonator are decoupled from each other.

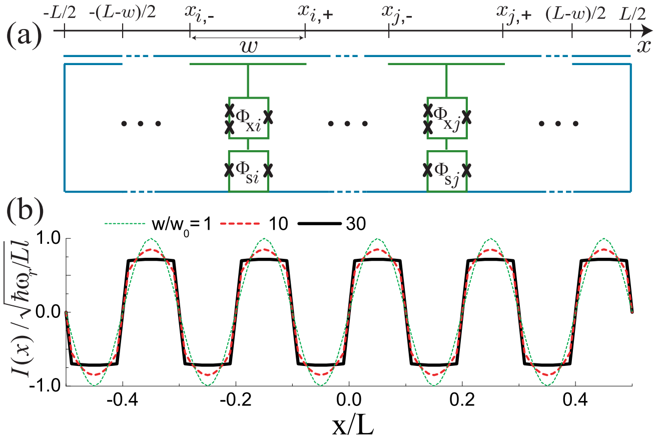

FIG. 4: (a) A schematic diagram for a scalable design of circuit QED with current-biased three-junctions flux qubits. Here we show, for example, two qubits and $x_{i,\pm}$ is given in Appendix A. The dc-SQUIDs between qubit and ground plane take the role of switching the coupling between qubit and resonator. The capacitance line has the width of w. (b) Current profiles when there are nine qubits in the circuit of (a) for $(d_0/d, w/w_0) = (1,1), (5,10), (15,30)$. The current gaps appear at qubit sites, and grow as the width w of capacitance line increases.

In Fig. 4(b) we show the current profiles in the resonator for 9 qubits. In this case we use the 10th harmonic mode of the resonator. Similarly to the single qubit case of Fig. 2(a) the current gap increases at the qubit sites along with w/w_0 and d_0/d. However, the coupling strength is different from that of the single qubit case.

If there are N qubits in the circuit, we need (N+1)th harmonic mode in the resonator. For large N we use higher resonator mode, and thus ω_r has larger value in Fig. 5(b). The higher mode has a shorter wave length, and thus larger amount of bias current flows from the capacitance line of width w to the qubit. As a result, the current gap δ becomes larger for many qubits [Fig. 5(a)]. Since both ω_r and δ have large values for many qubits in the circuit, the coupling g in Eq. (16) increases along with the number of qubits N [Fig. 5(c)]. Note that though the high frequency of resonator field might be technically challenging, the resonator frequency can

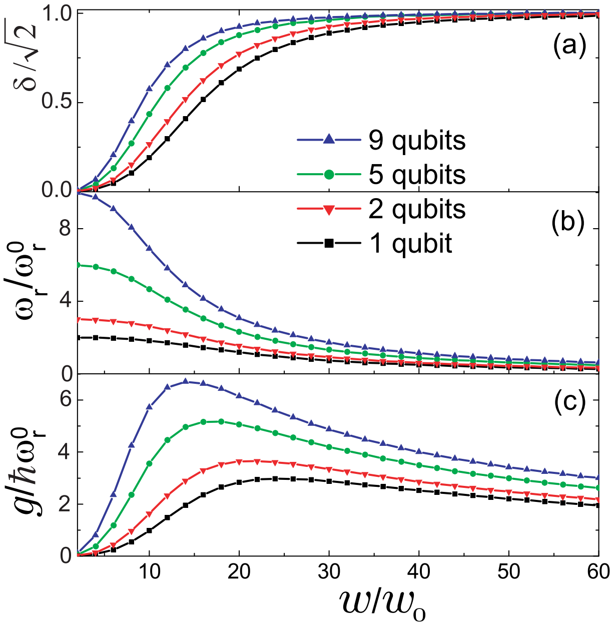

FIG. 5: (a) The current gap δ for N =1, 2, 5, 9 qubits in the circuit of Fig. 4 as a function of w/w_0 along the diagonal line $w/w_0 = 2d_0/d$ in the bottom of Fig. 3. $\delta/\sqrt{2}$ increases along with w/w_0 and saturate to 1 finally. (b) The resonator frequency w_r decreases as w/w_0 increases. As N increases, we need higher resonator mode and thus higher resonator frequency w_r. (c) The coupling constant g shows a maximum which is larger for more number of qubits.

be minimized, if we increase w/w_0 or d_0/d [Fig. 5(b)].

B. Two-qubit coupling

The universal gate in quantum computing requires a two-qubit gate in addition to the single qubit operation. In the scalable design of Fig. 4(a) the two-qubit Hamiltonian is given by

$$H_{2\mathrm{q}}= \omega_r a^\dagger a+\sum_{k=1,2}\frac{\omega_{ak}}{2}\sigma_{zk}-i\sum_{k=1,2} g_k(a^\dagger\sigma_{-k}-a\sigma_{+k}). \quad (21)$$

In the dispersive regime $|\Delta_k| = |\omega_{ak} - \omega_r| \gg g_k$, we can obtain the coupling Hamiltonian

$$H_{\mathrm{int}} = \frac{1}{2}\left(\frac{1}{\Delta_1}+\frac{1}{\Delta_2}\right) g_1 g_2(\sigma_{-1}\sigma_{+2} + \sigma_{+1}\sigma_{-2}) \quad (22)$$

by introducing a transformation similar to that in Ref. [2]

$$U_2 = e^{-i\frac{g_1}{\Delta_1}(a^\dagger\sigma_{-1}+a\sigma_{+1})-i\frac{g_2}{\Delta_2}(a^\dagger\sigma_{-2}+a\sigma_{+2})}. \quad (23)$$

When the qubit-resonator coupling g is strong, the Hamiltonian should be solved by exact diagonalization rather than by series expansion with a small parameter. The two-qubit Hamiltonian of Eq. (21) can be written as $H_{2\mathrm{q}} = H_{\mathrm{cavity}} \otimes H_{\mathrm{qubit1}} \otimes H_{\mathrm{qubit2}}$ and we introduce a transformation matrix

$$\mathcal{U}_2 = e^{-i\frac{\varphi_1}{\sqrt{2}}(a^\dagger\sigma_{-1}+a\sigma_{+1})-i\frac{\varphi_2}{\sqrt{2}}(a^\dagger\sigma_{-2}+a\sigma_{+2})} \quad (24)$$

in the same basis. Then the Hamiltonian H_{2q} and the transformation matrix $\mathcal{U}_2$ can be represented by a block-diagonal matrix by slightly changing the order of basis.

For simplicity, we consider nominally identical qubits, $\omega_{a1} = \omega_{a2}$, $g_1 = g_2$, and $\varphi_1 = \varphi_2$, and then the lowest block involving the resonator photon number $n = 0$ and 1 in the Hamiltonian is written as

$$H_{2\mathrm{q}} = \begin{pmatrix} -\Delta & -ig & -ig \\ ig & 0 & 0 \\ ig & 0 & 0 \end{pmatrix} \quad (25)$$

with the basis $\{|1\downarrow\downarrow\rangle, |0\uparrow\downarrow\rangle, |0\downarrow\uparrow\rangle\}$, where $|\uparrow\rangle$ and $|\downarrow\rangle$ are the qubit states, and $|0\rangle$ and $|1\rangle$ are the photon number states. Further the lowest block of the transformation matrix in the same basis can be evaluated by exactly summing a infinite series as

$$\mathcal{U}_2 = \begin{pmatrix} \cos\varphi & -\frac{i}{\sqrt{2}}\sin\varphi & -\frac{i}{\sqrt{2}}\sin\varphi \\ -\frac{i}{\sqrt{2}}\sin\varphi & \cos^2\frac{\varphi}{2} & -\sin^2\frac{\varphi}{2} \\ -\frac{i}{\sqrt{2}}\sin\varphi & -\sin^2\frac{\varphi}{2} & \cos^2\frac{\varphi}{2} \end{pmatrix}. \quad (26)$$

Then we can easily check that if the condition $\tan 2\varphi = 2\sqrt{2}g/\Delta$ is satisfied, the transformed Hamiltonian $\tilde{H}_{2\mathrm{q}} = \mathcal{U}_2^\dagger H_{2\mathrm{q}}\mathcal{U}_2$ becomes block-diagonal further as follows:

$$\tilde{H}_{2\mathrm{q}} = \begin{pmatrix} -\Delta-\sqrt{2}g\tan\varphi & 0 & 0 \\ 0 & \frac{g}{\sqrt{2}}\tan\varphi & \frac{g}{\sqrt{2}}\tan\varphi \\ 0 & \frac{g}{\sqrt{2}}\tan\varphi & \frac{g}{\sqrt{2}}\tan\varphi \end{pmatrix}, \quad (27)$$

which describes the xy-type coupling between two states, $|0\uparrow\downarrow\rangle$ and $|0\downarrow\uparrow\rangle$, with the coupling constant

$$J = \frac{g}{\sqrt{2}}\tan\varphi \quad (28)$$

for $n = 0$. J can be explicitly evaluated with above condition and the interaction Hamiltonian is written by

$$H_{\mathrm{int}} = \pm\frac{g^2}{\sqrt{\left(\frac{\Delta}{2}\right)^2+2g^2}+\frac{|\Delta|}{2}}(\sigma_{-1}\sigma_{+2}+\sigma_{+1}\sigma_{-2}), \quad (29)$$

where the sign is $+$ for $\Delta > 0$ and $-$ for $\Delta < 0$ because $g > 0$. For the two-qubit Hamiltonian with the transmon qubits $H_{2\mathrm{q}} = \omega_r a^\dagger a + \sum_{k=1,2}\frac{\omega_{ak}}{2}\sigma_{zk} - \sum_{k=1,2} g_k(a^\dagger\sigma_{-k} + \sigma_{+k}a)$, the same coupling constant J can be obtained by using the transformation matrix $U = e^{-\frac{\varphi_1}{\sqrt{2}}(a^\dagger\sigma_{-1}-a\sigma_{+1})-\frac{\varphi_2}{\sqrt{2}}(a^\dagger\sigma_{-2}-a\sigma_{+2})}$.

In Fig. 6(a) we show $|J|/\hbar\omega_r^0$ in the plane of $(d_0/d, w/w_0)$ when there are only two qubits in the circuit of Fig. 4. We set $\omega_a/2\pi$=2GHz for usual flux qubits, $\omega_r^0/2\pi$=6GHz,[9] and $Z = 50\Omega$.[6,10] The strong two-qubit coupling $J \sim \hbar\omega_r^0$ can be obtained with a few multiple

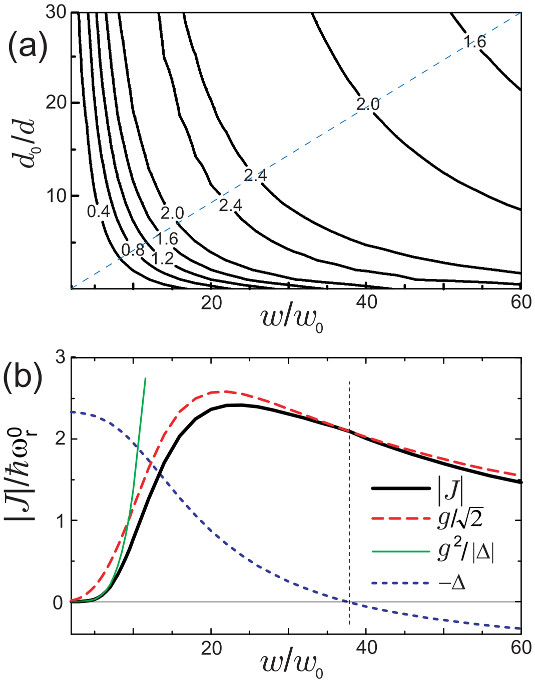

FIG. 6: (a) Contour plot for the two-qubit xy-type interaction strength $J/\hbar\omega_r^0$ in the plane of $(d_0/d, w/w_0)$ when there are only two qubits in the circuit. The parameter values are $Z = 50\Omega$, $\omega_r^0/2\pi$=6GHz, and $\omega_a/2\pi$=2GHz. (b) The two-qubit coupling $|J|$ along the dotted line in (a). For weak coupling $|J|$ scales as $g^2/|\Delta|$, while in the limit of large $g/|\Delta|$ $|J|$ approaches $g/\sqrt{2}$. At the point $w/w_0 \sim 38$, the sign of Δ changes, which implies the change from ferromagnetic to antiferromagnetic two-qubit coupling.

values of w_0 and $1/d_0$. The two-qubit coupling J also shows a maximum where $J/\hbar\omega_r^0 \sim 2.4$.

Fig. 6(b) shows the cut view of $|J|$ along the dotted line in (a). For small g/Δ limit the condition $\tan 2\varphi = 2\sqrt{2}g/\Delta$ is written as $\varphi \approx \sqrt{2}g/\Delta$. Then, the transformation matrix $\mathcal{U}_2$ in Eq. (24) is reduced to U_2 in Eq. (23), and the coupling constant $J = \frac{g}{\sqrt{2}}\tan\varphi$ becomes $J \approx g^2/\Delta$ in accordance with Eq. (22). For large g/Δ limit, J is given by $J \approx \pm g/\sqrt{2}$.

These behaviors are demonstrated in Fig. 6(b). For small w/w_0 where the coupling g is weak, it is shown that $J \sim g^2/\Delta$. As w/w_0 grows, Δ increases because ω_r in Fig. 5(b) decreases. At the point where the sign of Δ changes, g/Δ goes to infinity and J approaches $\pm g/\sqrt{2}$. Hence, by changing parameters $(w/w_0, d_0/d)$ around this point the two-qubit ferromagnetic or antiferromagnetic xy-type interaction can be obtained selectively.

IV. SUMMARY

In summary, we propose a circuit QED architecture with current-biased flux qubits. The three-junctions flux qubit is coupled with the resonator by a bias current flowing through the capacitance between the qubit and the resonator. We introduce a capacitance line extended from the qubit loop which takes the role of leading the oscillating current, flowing from the resonator to the ground plane, into the qubit loop. For much larger capacitance almost current flows through the qubit, resulting in a ultrastrong coupling between the qubit and the resonator.

The two-qubit xy-type interaction also can reach strong coupling regime owing to the strong qubit-resonator coupling. Hence the two-qubit gate will be performed sufficiently fast in a finite coherence time of the flux qubit. The two-qubit gate in a scalable design can be performed by introducing dc-SQUIDs between the qubit and the ground plane to switch on/off the qubit-resonator coupling. We provide an exact expression of the two-qubit coupling which shows the transition from ferromagnetic to antiferromagnetic two-qubit coupling in circuit QED with the current-biased flux qubits.

ACKNOWLEDGMENTS

The author acknowledges the useful discussion with K. Moon. This research was supported by Basic Science Research Program through the National Research Foundation of Korea (NRF) funded by the Ministry of Education, Science and Technology (2011-0023467).

---

[1] A. Blais, R.-S. Huang, A. Wallraff, S. M. Girvin, and R. J. Schoelkopf, Phys. Rev. A **69**, 062320 (2004).

[2] A. Blais, J. Gambetta, A. Wallraff, D. I. Schuster, S. M. Girvin, M. H. Devoret, and R. J. Schoelkopf, Phys. Rev. A **75**, 032329 (2007).

[3] J. E. Mooij, T. P. Orlando, L. Levitov, L. Tian, C. H. van der Wal, and S. Lloyd, Science **285**, 1036 (1999); I. Chiorescu, Y. Nakamura, C. J. P. M. Harmans, and J. E. Mooij, Science **299**, 1869 (2003).

[4] T. P. Orlando, J. E. Mooij, L. Tian, C. H. van der Wal, L. S. Levitov, Seth Lloyd, and J. J. Mazo, Phys. Rev. B **60**, 15398 (1999).

[5] M. D. Kim, D. Shin, and J. Hong, Phys. Rev. B **68**, 134513 (2003).

[6] A. A. Abdumalikov, Jr., O. Astafiev, Y. Nakamura, Y. A. Pashkin, and J. S. Tsai, Phys. Rev. B **78**, 180502(R) (2008); J. Bourassa, J. M. Gambetta, A. A. Abdumalikov, Jr., O. Astafiev, Y. Nakamura, and A. Blais, Phys. Rev. A **80**, 032109 (2009).

[7] T. Niemczyk, F. Deppe, H. Huebl, E. P. Menzel, F. Hocke, M. J. Schwarz, J. J. Garcia-Ripoll, D. Zueco, T. Hummer, E. Solano, A. Marx, and R. Gross, Nature Phys. **6**, 772 (2010).

[8] A. Fedorov, A. K. Feofanov, P. Macha, P. Forn-Díaz, C. J. P. M. Harmans, and J. E. Mooij, Phys. Rev. Lett. **105**, 060503 (2010).

[9] T. Lindstrom, C. H. Webster, J. E. Healey, M. S. Colclough, C. M. Muirhead, and A. Y. Tzalenchuk, Supercond. Sci. Technol. **20**, 814 (2007).

[10] G. Oelsner, S. H. W. van der Ploeg, P. Macha, U. Hubner, D. Born, S. Anders, E. Il'ichev, H.-G. Meyer, M. Grajcar, S. Wünsch and M. Siegel, A. N. Omelyanchouk, and O. Astafiev Phys. Rev. B **81**, 172505 (2010).

[11] J. M. Martinis, S. Nam, J. Aumentado, and C. Urbina, Phys. Rev. Lett. **89**, 117901 (2002).

[12] J. M. Martinis, Quant. Inform. Proc. **8**, 81 (2009).

[13] A. J. Berkley, H. Xu, R. C. Ramos, M. A. Gubrud, F. W. Strauch, P. R. Johnson, J. R. Anderson, A. J. Dragt, C. J. Lobb, and F. C. Wellstood, Science **300**, 1548 (2003).

[14] M. A. Sillanpää, J. I. Park, and R. W. Simmonds, Nature **449**, 438 (2007).

[15] M. D. Kim and K. Moon, J. Korean Phys. Soc. **58**, 1599 (2011); arXiv: 1005.1703.

[16] See, e.g., M. Tinkham, *Introduction to Superconductivity* (McGraw Hill, New York, ed. 2, 1996).

[17] M. Steffen, S. Kumar, D. P. DiVincenzo, J. R. Rozen, G. A. Keefe, M. B. Rothwell, and M. B. Ketchen, Phys. Rev. Lett. **105**, 100502 (2010).

[18] J. M. Chow, A. D. Corcoles, J. M. Gambetta, C. Rigetti, B. R. Johnson, J. A. Smolin, J. R. Rozen, G. A. Keefe, M. B. Rothwell, M. B. Ketchen, and M. Steffen, Phys. Rev. Lett. **107**, 080502 (2011).

[19] K. Inomata, T. Yamamoto, P.-M. Billangeon, Y. Nakamura, and J. S. Tsai, Phys. Rev. B **86**, 140508(R) (2012).

[20] R.-S. Huang, PhD thesis, Indiana Univ. (2004).

Appendix A: N qubits

Let's first consider the case that the number of qubit N is odd. Then the spatial part $X(x)$ of the wavefunction is written by

$$X(x)=\begin{cases} A_{-N-1}e^{i\frac{j_2\pi}{L}x}+B_{-N-1}e^{-i\frac{j_2\pi}{L}x} & (-\frac{L}{2}<x<-\frac{L}{2}+\frac{w}{2}) \\ \quad\cdot & \\ \quad\cdot & \\ \quad\cdot & \\ A_{k_o}e^{-i\frac{j_1\pi}{L}x}+B_{k_o}e^{-i\frac{j_1\pi}{L}x} & (x_{k_o-1,+}<x<x_{k_o+1,-}) \\ A_{k_e}e^{-i\frac{j_2\pi}{L}x}+B_{k_e}e^{-i\frac{j_2\pi}{L}x} & (x_{k_e-}<x<x_{k_e+}) \\ \quad\cdot & \\ \quad\cdot & \\ \quad\cdot & \\ A_{N+1}e^{i\frac{j_2\pi}{L}x}+B_{N+1}e^{-i\frac{j_2\pi}{L}x} & (\frac{L}{2}-\frac{w}{2}<x<\frac{L}{2}), \end{cases} \tag{A1}$$

where k_e is even and k_o is odd among $k = 0, \pm1, \pm2, ..., \pm(N+1)$. Here $x_{k_e\pm} = \frac{k_e}{N+1}\frac{L}{2} \pm \frac{w}{2}$, $x_{k_o\pm1,\pm} = \frac{k_o\pm1}{N+1}\frac{L}{2} \pm \frac{w}{2}$, $x_{-N-1,-} = -\frac{L}{2}$, and $x_{N+1,+} = \frac{L}{2}$.

The conditions for continuity of $X(x)$ are given by

$$\begin{aligned} &A_{k_o-1}e^{i\frac{j_2\pi}{L}x_{k_o-1,+}}+B_{k_o-1}e^{-i\frac{j_2\pi}{L}x_{k_o-1,+}} \\ &= A_{k_o}e^{i\frac{j_1\pi}{L}x_{k_o-1,+}}+B_{k_o}e^{-i\frac{j_1\pi}{L}x_{k_o-1,+}} \end{aligned} \tag{A2}$$

$$\begin{aligned} &A_{k_e-1}e^{i\frac{j_1\pi}{L}x_{k_e-}}+B_{k_e-1}e^{-i\frac{j_1\pi}{L}x_{k_e-}} \\ &= A_{k_e}e^{i\frac{j_2\pi}{L}x_{k_e-}}+B_{k_e}e^{-i\frac{j_2\pi}{L}x_{k_e-}} \end{aligned} \tag{A3}$$

with $k = 0, \pm1, \pm2, ..., \pm N, N+1$, and the boundary conditions at the end of resonator are

$$A_{-N-1}e^{-i\frac{j_2\pi}{2}}+B_{-N-1}e^{i\frac{j_2\pi}{2}}=0, \tag{A4}$$

$$A_{N+1}e^{i\frac{j_2\pi}{2}}+B_{N+1}e^{-i\frac{j_2\pi}{2}}=0. \tag{A5}$$

Eq. (A2) can be written in terms of k_e and Eq. (A3) in terms of k_o. If we set $k_e = -k_o+1$ and use the relation $x_{-k,\pm} = -x_{k,\mp}$, Eqs. (A2) and (A3) becomes

$$\begin{aligned} &A_{-k_e}e^{-i\frac{j_2\pi}{L}x_{k_e-}}+B_{-k_e}e^{i\frac{j_2\pi}{L}x_{k_e-}} \\ &= A_{-k_e+1}e^{-i\frac{j_1\pi}{L}x_{k_e-}}+B_{-k_e+1}e^{i\frac{j_1\pi}{L}x_{k_e-}}, \end{aligned} \tag{A6}$$

$$\begin{aligned} &A_{-k_o}e^{-i\frac{j_1\pi}{L}x_{k_o-1,+}}+B_{-k_o}e^{i\frac{j_1\pi}{L}x_{k_o-1,+}} \\ &= A_{-k_o+1}e^{-i\frac{j_2\pi}{L}x_{k_o-1,+}}+B_{-k_o+1}e^{i\frac{j_2\pi}{L}x_{k_o-1,+}}, \end{aligned} \tag{A7}$$

respectively.

A set of boundary conditions is obtained from sum of Eqs. (A3) and (A6), Eqs. (A2) and (A7), and Eqs. (A4) and (A5) as follows:

$$\begin{aligned} &(A_{-k_e}+B_{k_e})e^{-i\frac{j_2\pi}{L}x_{k_e-}}+(A_{k_e}+B_{-k_e})e^{i\frac{j_2\pi}{L}x_{k_e-}} \\ &=(A_{-k_e+1}+B_{k_e-1})e^{-i\frac{j_1\pi}{L}x_{k_e-}}+(A_{k_e-1}+B_{-k_e+1})e^{i\frac{j_1\pi}{L}x_{k_e-}}, \end{aligned} \tag{A8}$$

$$\begin{aligned} &(A_{-k_o}+B_{k_o})e^{-i\frac{j_1\pi}{L}x_{k_o-1,+}}+(A_{k_o}+B_{-k_o})e^{i\frac{j_1\pi}{L}x_{k_o-1,+}} \\ &=(A_{-k_o+1}+B_{k_o-1})e^{-i\frac{j_2\pi}{L}x_{k_o-1,+}}+(A_{k_o-1}+B_{-k_o+1})e^{i\frac{j_2\pi}{L}x_{k_o-1,+}}, \end{aligned} \tag{A9}$$

$$(A_{N+1}+B_{-N-1})e^{i\frac{j_2\pi}{2}}+(A_{-N-1}+B_{N+1})e^{-i\frac{j_2\pi}{2}}=0. \tag{A10}$$

From the condition for continuity of $(1/c_i)dX_i(x)/dx$ similar equations are also obtained as

$$\begin{aligned} &-\frac{j_2}{c'}(A_{-k_e}+B_{k_e})e^{-i\frac{j_2\pi}{L}x_{k_e-}}+\frac{j_2}{c'}(A_{k_e}+B_{-k_e})e^{i\frac{j_2\pi}{L}x_{k_e-}} \\ &= -\frac{j_1}{c}(A_{-k_e+1}+B_{k_e-1})e^{-i\frac{j_1\pi}{L}x_{k_e-}} \\ &\quad + \frac{j_1}{c}(A_{k_e-1}+B_{-k_e+1})e^{i\frac{j_1\pi}{L}x_{k_e-}}, \end{aligned} \tag{A11}$$

$$\begin{aligned} &-\frac{j_1}{c}(A_{-k_o}+B_{k_o})e^{-i\frac{j_1\pi}{L}x_{k_o-1,+}}+\frac{j_1}{c}(A_{k_o}+B_{-k_o})e^{i\frac{j_1\pi}{L}x_{k_o-1,+}} \\ &= -\frac{j_2}{c'}(A_{-k_o+1}+B_{k_o-1})e^{-i\frac{j_2\pi}{L}x_{k_o-1,+}} \\ &\quad + \frac{j_2}{c'}(A_{k_o-1}+B_{-k_o+1})e^{i\frac{j_2\pi}{L}x_{k_o-1,+}}. \end{aligned} \tag{A12}$$

The boundary conditions of Eqs. (A8)-(A12) are represented in terms of $A_{-k}+B_k$. On the other hand, another set of boundary conditions can be obtained in terms of $A_{-k}-B_k$ as follows:

$$\begin{aligned} &(A_{-k_e}-B_{k_e})e^{-i\frac{j_2\pi}{L}x_{k_e-}}-(A_{k_e}-B_{-k_e})e^{i\frac{j_2\pi}{L}x_{k_e-}} \\ &=(A_{-k_e+1}-B_{k_e-1})e^{-i\frac{j_1\pi}{L}x_{k_e-}}-(A_{k_e-1}-B_{-k_e+1})e^{i\frac{j_1\pi}{L}x_{k_e-}}, \end{aligned} \tag{A13}$$

$$\begin{aligned} &(A_{-k_o}-B_{k_o})e^{-i\frac{j_1\pi}{L}x_{k_o-1,+}}-(A_{k_o}-B_{-k_o})e^{i\frac{j_1\pi}{L}x_{k_o-1,+}} \\ &=(A_{-k_o+1}-B_{k_o-1})e^{-i\frac{j_2\pi}{L}x_{k_o-1,+}}-(A_{k_o-1}-B_{-k_o+1})e^{i\frac{j_2\pi}{L}x_{k_o-1,+}}, \end{aligned} \tag{A14}$$

$$(A_{N+1}-B_{-N-1})e^{i\frac{j_2\pi}{2}}-(A_{-N-1}-B_{N+1})e^{-i\frac{j_2\pi}{2}}=0, \tag{A15}$$

$$\begin{aligned} &-\frac{j_2}{c'}(A_{-k_e}-B_{k_e})e^{-i\frac{j_2\pi}{L}x_{k_e-}}-\frac{j_2}{c'}(A_{k_e}-B_{-k_e})e^{i\frac{j_2\pi}{L}x_{k_e-}} \\ &= -\frac{j_1}{c}(A_{-k_e+1}-B_{k_e-1})e^{-i\frac{j_1\pi}{L}x_{k_e-}} \\ &\quad - \frac{j_1}{c}(A_{k_e-1}-B_{-k_e+1})e^{i\frac{j_1\pi}{L}x_{k_e-}}, \end{aligned} \tag{A16}$$

$$\begin{aligned} &-\frac{j_1}{c}(A_{-k_o}-B_{k_o})e^{-i\frac{j_1\pi}{L}x_{k_o-1,+}}-\frac{j_1}{c}(A_{k_o}-B_{-k_o})e^{i\frac{j_1\pi}{L}x_{k_o-1,+}} \\ &= -\frac{j_2}{c'}(A_{-k_o+1}-B_{k_o-1})e^{-i\frac{j_2\pi}{L}x_{k_o-1,+}} \\ &\quad - \frac{j_2}{c'}(A_{k_o-1}-B_{-k_o+1})e^{i\frac{j_2\pi}{L}x_{k_o-1,+}}. \end{aligned} \tag{A17}$$

As a result, there are two sets of boundary conditions of (i) Eqs. (A8)-(A12) and (ii) Eqs. (A13)-(A17). Each set can be treated as an independent eigenvalue problem. If the determinant of matrix corresponding to set (i) is non-zero while that for (ii) is zero, we have $A_{-k} = -B_k$. Around the central qubit site the solution becomes $X_0(x) \sim A_0 \sin\frac{j_2\pi}{L}x$. On the contrary, if the determinant for (i) is zero while that for (ii) is non-zero, we have $A_{-k} = B_k$ and $X_0(x) \sim A_0 \cos\frac{j_2\pi}{L}x$. For the case that the number of qubits N is even, a similar analysis can also be performed.